Wideband Integrated Quad-Element MIMO Antennas Based on Complementary Antenna Pairs for 5G Smartphones

Libin Sun, *Graduate Student Member, IEEE*, Yue Li, *Senior Member, IEEE*, and Zhijun Zhang, *Fellow, IEEE*

***Abstract*— In this article, a wideband and highly-integrated quad-element multiple-input multiple-output (MIMO) antenna is proposed for the first time, to adapt to the size-limited environment in fifth-generation (5G) smartphones. First, the wideband decoupling between two extremely closely-spaced open-slot antennas with face-to-face and back-to-back configurations are investigated. Then, based on the complementary antenna pairs, wideband integrated quad-element MIMO antennas are implemented by the ingenious combination of these antenna pairs. For validation, an 8 × 8 MIMO system, constituted by two sets of integrated quad-antenna configurations, is simulated, fabricated, and measured. Both the simulated and measured results show that the 8 × 8 MIMO system can provide isolation of better than 10 dB between any two ports and a total antenna efficiency of 52.8%–70.8%/40.5%–75.0% across 3.3–5.0 GHz. Compared with the existing integrated quad-antenna design schemes, the proposed solution can expand the bandwidth from less than 200 to 1700 MHz, covering the entire 5G N77, N78, and N79 bands. In addition to the integrated quad-antenna design, further extension to integrated multiantenna configurations is also discussed by the flexible combination of complementary antenna pairs, which paves the way for future higher-order MIMO system in smartphones.**

***Index Terms*— Antenna diversity, decoupling, fifth-generation (5G), integrated multiantenna, multiple-input multiple-output (MIMO), smartphone antenna.**

I. Introduction

MASSIVE multiple-input and multiple-output (MIMO) has been validated as an essential technique of fifth-generation (5G) communication systems [1]. The channel capacity for 5G can be enhanced once a large number of antennas are available at base stations and mobile terminals [2]. Generally, about 4–8 MIMO antennas operating at sub-6 GHz spectrum are demanded in 5G mobile terminals to enhance the throughput rate of users [3]–[17]. However, with the full-screen development trend of the up-to-date smartphones, the area and ground clearance reserved for antenna design are extremely squeezed [18]–[20]. Therefore, advanced decoupling techniques and integrated MIMO antenna design schemes should be investigated to minimize the space allocation of multiple co-frequency antennas for accommodating the ongoing 5G evolution.

Recently, some integrated yet decoupled dual-antenna pairs with various decoupling techniques have been proposed to reduce the space allocation [21]–[40]. In [21] and [22], two closely-spaced gap-coupled loop antennas are integrated as a building block with an internal coupling cancellation. Parasitic grounded strips are employed in [23]–[26] to cancel the mutual coupling between two closely-spaced antennas by the extra coupling path. In [27] and [28], lumped components are utilized to build an *LC* tank between closely-spaced antenna elements for the coupling suppression. The physical orthogonality can also be used to design integrated antenna pairs with natural high isolation. Orthogonal monopole and dipole antenna pairs [29]–[32], slot and open-slot antenna pairs [33], [34], monopole and loop antenna pairs [35], and monopole and open-slot antenna pairs [36], [37] are investigated to achieve isolation of above 20 dB even in the closely-spaced configuration. And the bandwidth of the orthogonal-mode antenna pair can be further enhanced by the combination of two sets of orthogonal modes at different bands [38]. Recently, a mode cancellation method is also proposed to design shared-radiator antenna pairs [39], [40] across a wide bandwidth.

The above-mentioned integrated MIMO antenna design schemes are only limited to the decoupling between two elements, and can hardly be extended to more elements. To further increase the integration level, integrated quad-element MIMO antennas are presented in [41] and [42]. In [41], four open-slot antennas are configured into a linear array and decoupled by three neutralization lines at 3.4–3.6 GHz. However, the distance between two central elements is large, thereby expanding its overall size. In [42], four tightly-arranged inverted-F antennas (IFAs) are integrated and decoupled by three lumped components at 3.6–3.735 GHz. The integrated quad-element design schemes can dramatically reduce the space allocation of 5G antennas; however, the narrow bandwidth of the existing design schemes cannot meet the requirement of global 5G bands: N77 (3.3–4.2 GHz), N78 (3.3–3.8 GHz), and N79 (4.4–5.0 GHz). In addition, the metal frame in mainstream smartphones is also not considered in the

Manuscript received October 4, 2020; revised December 8, 2020; accepted December 30, 2020. Date of publication February 24, 2021; date of current version August 4, 2021. This work was supported in part by the National Natural Science Foundation of China under Contract 61971254, and in part by Huawei Terminal Company, Ltd. *(Corresponding author: Zhijun Zhang.)*

The authors are with the Beijing National Research Center for Information Science and Technology (BNRist), Tsinghua University, Beijing, 100084, China (e-mail: zjzh@tsinghua.edu.cn).

Color versions of one or more figures in this article are available at https://doi.org/10.1109/TAP.2021.3060020.

Digital Object Identifier 10.1109/TAP.2021.3060020

design of the integrated quad-element MIMO antennas in [41] and [42].

To address the bandwidth limitation of the highly-integrated quad-element MIMO antennas, here, a wideband quad-element MIMO antenna co-designed with the metal frame of 5G smartphones is proposed for the first time. First, the wideband decoupling between two closely-spaced open-slot antennas with face-to-face and back-to-back configurations is investigated. Then, by the combination of the complementary antenna pairs, integrated quad-element MIMO antennas can be constructed. Compared with the existing integrated quad-antenna design schemes, the proposed solution can expand the operating bandwidth from less than 200 [41], [42] to 1700 MHz, covering the entire 5G N77, N78, and N79 bands. In addition to the integrated quad-antenna design, further extension to integrated multiantenna design can also be realized through the flexible combination of the complementary antenna pairs, which paves the way for future higher-order MIMO systems in smartphones.

This article is organized as follows. In Section II, the wideband decoupling of complementary open-slot antenna pairs with face-to-face and back-to-back configurations is investigated. In Section III, the evolution process of the integrated quad-element MIMO antenna is illustrated, and then, an 8 × 8 MIMO antenna system constituted by two sets of quad-element MIMO antennas is simulated, fabricated, and measured. In Section IV, the impact of the user's hand in practical application scenarios is discussed. In Section V, a further extension to the integrated multiantenna configuration is investigated. Finally, Section VI draws a conclusion.

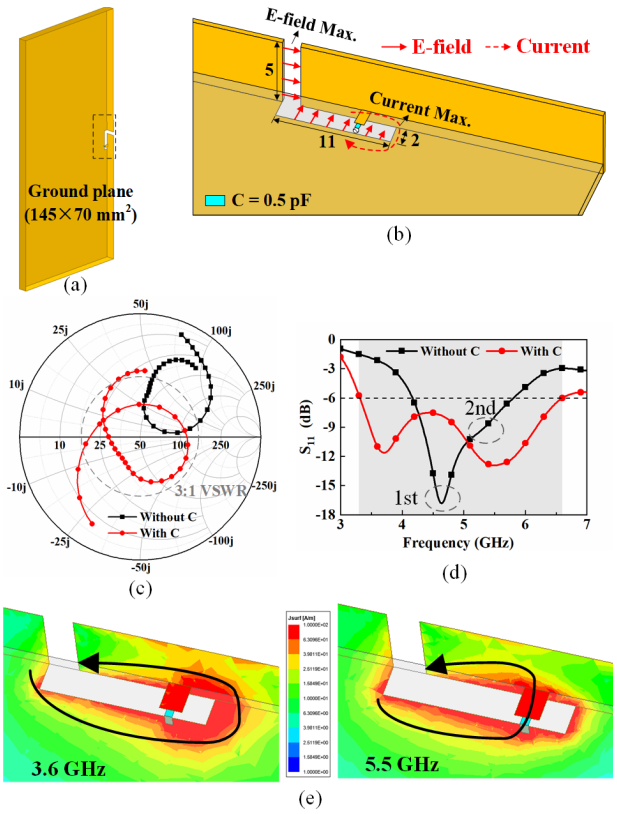

Fig. 1. (a) Geometry of the open-slot antenna designed in a metal frame smartphone casing. (b) Detailed structure of the open-slot antenna element, unit all in millimeters. (c) Simulated Smith chart of S_{11} with and without the matching capacitance (frequency span: 3.0–7.0 GHz). (d) Simulated S_{11} with and without the matching capacitance. (e) Simulated current distributions at two resonant frequencies of the matched open-slot antenna.

II. Wideband Complementary Antenna Pairs

A. Open-Slot Antenna Element

The open-slot antenna is widely used in smartphones because it could effectively excite the current in the ground plane and metal frame, thereby increasing the antenna bandwidth [14]. Fig. 1(a) shows the geometry of an L-shaped folded open-slot antenna designed in a metal frame smartphone casing. An FR-4 substrate ($\varepsilon_r = 4.4$, $\tan\delta = 0.02$), with a dimension of 145 × 70 × 0.8 mm^3, is used as the system mainboard. And a ground plane is printed at the bottom surface of the FR-4 substrate. A full circle of metal frame, with a height of 5 mm, is vertically surrounded and connected with the ground plane. As shown in Fig. 1(b), an 11 × 2 mm^2 slot is etched in the ground plane and a 5 × 2 mm^2 slot is etched in the metal frame to form an L-shaped open-slot antenna structure. The open-slot antenna has a maximum E-field at the open end and a maximum current at the short end as illustrated in Fig. 1(b). As shown in Fig. 1(c) and (d), if without the matching component, the impedance matching and bandwidth of the open-slot antenna are not very good due to the large inductance introduced from the feeding strip. To optimize the impedance matching, a 0.5 pF capacitance is connected in series in the feeding strip. As shown in Fig. 1(c), the series capacitance can move the antenna impedance downward from the inductive region to the capacitive region along the constant resistance circle [43]. Therefore, as shown in Fig. 1(d), a wide −6 dB impedance bandwidth of 3.3–3.6 GHz (2:1) with dual-resonance response can be realized for the proposed compact open-slot antenna element. To offer an intuitive view of the two resonant frequencies, the current distributions at two resonant frequencies are proposed in Fig. 1(e). As seen, at the first resonant frequency, the resonant mode is a full-length open-slot mode with a current maximum at the short end, whereas at the second resonant frequency, the resonant mode is a partial-length open-slot mode with a current maximum at the feeding strip.

B. Antenna Pair With Face-to-Face Configuration

When we put two closely-spaced L-shaped open-slot antenna elements together, an open-slot antenna pair can be formed as shown in Fig. 2(a). The array arrangement with adjacent short-circuit ends is defined as "face-to-face" configuration. Since the distance between the maximum current points of two antenna elements is only 1.5 mm, strong current coupling occurs between them. To suppress the coupling, a lumped capacitance C_d is inserted in the center grounded strip as shown in Fig. 2(b). To demonstrate the decoupling mechanism, an equivalent circuit of the decoupling structure is proposed in Fig. 2(c). The center grounded strip can be equivalent to an inductance, which can form a series LC tank with the inserted lumped capacitance. Under the ideal lossless

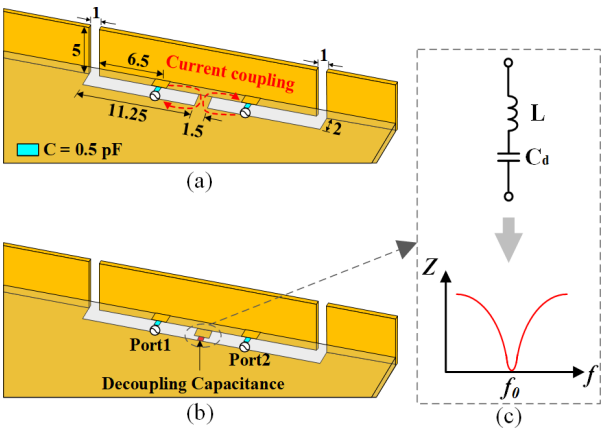

Fig. 2. (a) Two closely-spaced open-slot antennas as an antenna pair with face-to-face configuration (note that the antenna pair is also placed in the same metal frame smartphone casing, which is not shown for brevity), unit all in millimeter. (b) Lumped capacitance C_d (1.5 pF) is inserted in the center grounded strip for decoupling. (c) Equivalent circuit of the decoupling structure.

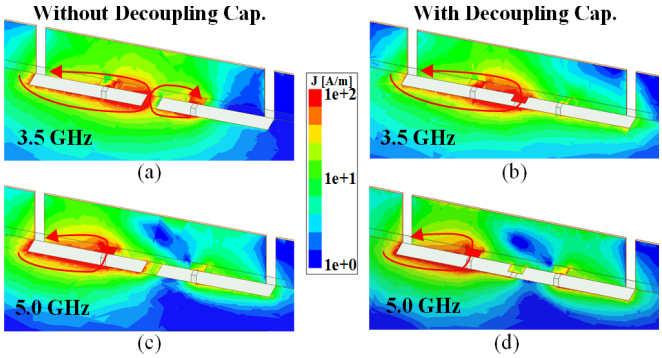

Fig. 3. Simulated current distribution of the face-to-face antenna pair when fed through port1. (a) Without and (b) with the decoupling capacitance at 3.5 GHz. (c) Without and (d) with the decoupling capacitance at 5.0 GHz.

condition, the series LC tank has zero input impedance at the resonant frequency ω_0 [44]

$$Z = j\omega_0 L + 1/j\omega_0 C_d = 0 \tag{1}$$

where

$$\omega_0 = 1/\sqrt{LC_d}. \tag{2}$$

Therefore, the strong coupling current between two antenna elements can be "short-circuited" by the series LC tank in the lower band, as shown in Fig. 3(a) and (b). In the higher band, as shown in Fig. 3(c) and (d), the resonant length of the open-slot element is not from the open end to the short end, but from the open end to the feeding point; therefore, the distance between two open-slot elements can be enlarged, which contributes to natural good isolation in the higher band. Hence, a wideband decoupling performance can be implemented.

The simulated S-parameters of the antenna pair without and with the decoupling capacitance are proposed in Fig. 4. With the help of the decoupling capacitance, the poor isolation in the lower band can be improved to 34 dB at 3.5 GHz and above 10 dB across the entire band, whereas the good isolation in the higher band almost remains unchanged. Meanwhile, the impedance matching is almost not affected

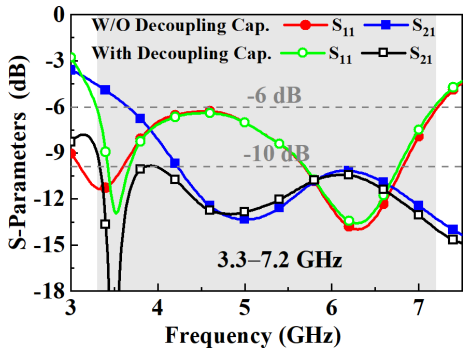

Fig. 4. Simulated S-parameters of the face-to-face antenna pair without and with the decoupling capacitance.

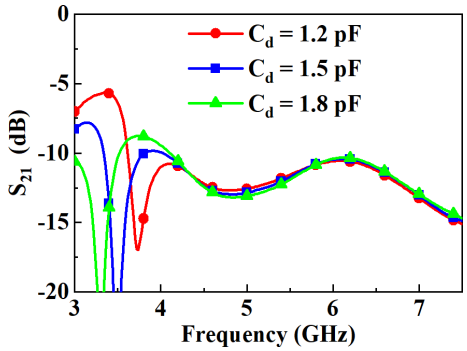

Fig. 5. Simulated S_{21} with different values of decoupling capacitance.

by the decoupling component. Consequently, an ultra-wide bandwidth of 3.3–7.2 GHz is realized with $S_{11} < -6$ dB and $S_{21} < -10$ dB, which exhibits a superior bandwidth performance compared with the existing integrated antenna pair solutions [21]–[40]. The isolation with different values of decoupling capacitance is presented in Fig. 5. As seen, with the increasing of the capacitance value, the lower-band decoupling frequency will be decreased, while the decoupling performance in the higher band keeps unchanged. Hence, the optimized decoupling capacitance value is 1.5 pF in this design.

To evaluate the radiation and diversity performance of the proposed antenna pair, the simulated antenna total efficiency and envelope correlation coefficient (ECC) is proposed in Fig. 6. The simulated antenna efficiency is 56.0%–88.0% across 3.3–7.2 GHz with an average value of 71.2%. The ECC is calculated by the simulated far-field [45], which is below 0.2 across the entire operating band and satisfies the standard in smartphones.

To highlight the advantages of the proposed design scheme, we compare this design with other integrated antenna pairs in 5G smartphones, as shown in Table I. The bandwidth of references [21], [23], [29], and [33] is only 3.4–3.6 GHz, which is too narrow to fit the global 5G spectrum. In [25] and [26], two wideband antenna pairs are proposed, but they cannot be applied in mainstream metal frame smartphones. In [38] and [40], two integrated antenna pairs co-designed with the metal frame are presented, but the antenna size is larger and the bandwidth is narrower than our design scheme. Therefore, the proposed design scheme promotes the miniaturization and wideband of integrated 5G antenna pairs.

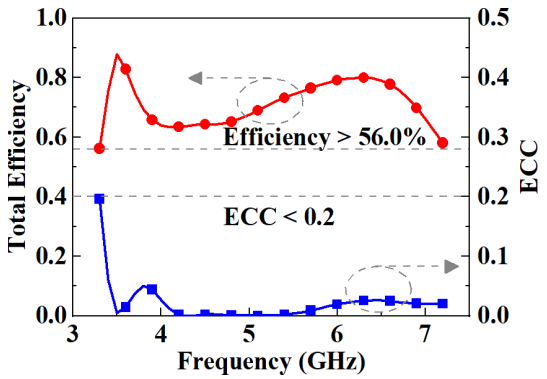

Fig. 6. Simulated efficiency and ECC of the face-to-face antenna pair.

TABLE I
COMPARISON OF THE INTEGRATED ANTENNA PAIRS FOR 5G SMARTPHONES

Ref	Metal Frame	Ant. Pair Size (mm^3)	Bandwidth* (GHz)	Isolation
[21]	×	10×1×7	3.4~3.6	>10 dB
[23]	×	20×1.8×7	3.4~3.6	>17 dB
[25]	×	35×1×7	3.3~6.0	>12 dB
[26]	×	28×1×5	3.3~6.0	>10 dB
[29]	×	12×1.8×7	3.4~3.6	>20 dB
[33]	√	25×1.5×7	3.4~3.6	>20 dB
[38]	√	40×3×7.5	3.3~5.0	>21 dB
[40]	√	28×1.8×7	3.3~5.0	>10 dB
Our work	√	24×2×5	3.3~7.2	>10 dB

* Overlapping bandwidth of S_{11} < -6 dB and S_{21} < -10 dB.

C. Back-to-Back Configuration

Alternatively, when we put two closely-spaced L-shaped open-slot antenna elements together by adjacent open ends, an integrated back-to-back open-slot antenna pair can be constructed as shown in Fig. 7(a). Compared with the face-to-face antenna pair, the back-to-back antenna pair shares one frame slot, thereby reducing the number of gaps in the metal frame of smartphones, which is more practical in engineering for achieving an exquisite industrial design. However, since two antenna elements share the maximum *E*-field point, strong *E*-field coupling occurs. Complementary to the face-to-face antenna pair, we can suppress the coupling of the back-to-back antenna pair by inserting a lumped inductance as shown in Fig. 7(b). The inserted inductance, combined with the parasitic capacitance of the frame slot, can construct a parallel *LC* tank. Under the ideal lossless condition, the parallel *LC* tank has an infinity input impedance at the resonant frequency [44], thereby blocking the in-between *E*-field coupling. However, the decoupling bandwidth is not sufficient due to the initial strong coupling in both lower and higher bands for this configuration [40]. Therefore, as shown in Fig. 7(c), an improved decoupling structure of connecting line is proposed in [40] to achieve a dual-mode decoupling in different bands. A wide decoupling bandwidth of 3.3–5.0 GHz can be realized by the novel decoupling structure. The detailed performance of the back-to-back open-slot antenna pair has been discussed in [40], which is not described in detail in this article.

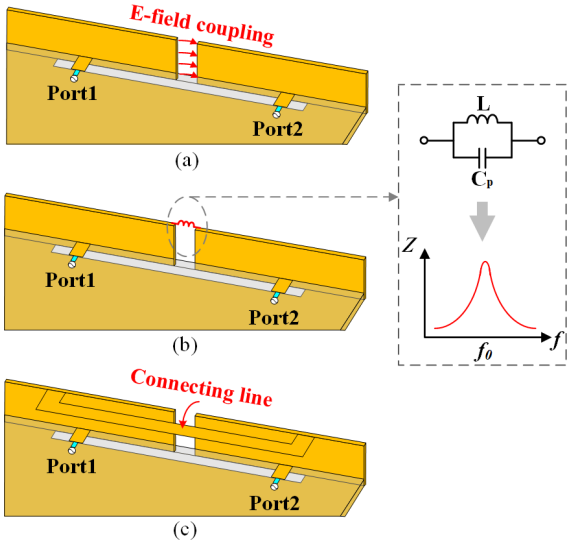

Fig. 7. (a) Integrated open-slot antenna pair with back-to-back configuration. (b) Back-to-back open-slot antenna pair decoupled by a center inductance. Inset is the equivalent circuit of the decoupling structure. (c) Back-to-back open-slot antenna pair decoupled by a connecting line [40].

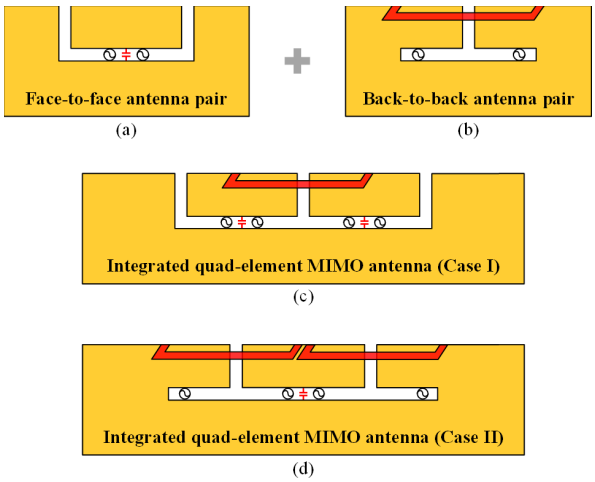

Fig. 8. Conceptual diagram: evolution process of the integrated quad-element MIMO antennas. (a) Face-to-face open-slot antenna pair. (b) Back-to-back open-slot antenna pair. (c) Integrated quad-element MIMO antenna (Case I). (d) Integrated quad-element MIMO antenna (Case II).

III. INTEGRATED QUAD-ELEMENT MIMO ANTENNAS

A. Evolution Process

Up to now, as shown in Fig. 8(a) and (b), the wideband decoupling of integrated antenna pairs with face-to-face and back-to-back configurations has been realized. The two antenna pairs have a complementary element arrangement, which is essential for the realization of the integrated quad-element antenna. When we put two sets of face-to-face antenna pairs together, the arrangement of two central elements is exactly the back-to-back configuration, so we can suppress the coupling between two central elements through a connecting line, as shown in Fig. 8(c). Consequently, an integrated quad-element configuration is realized, which is defined as

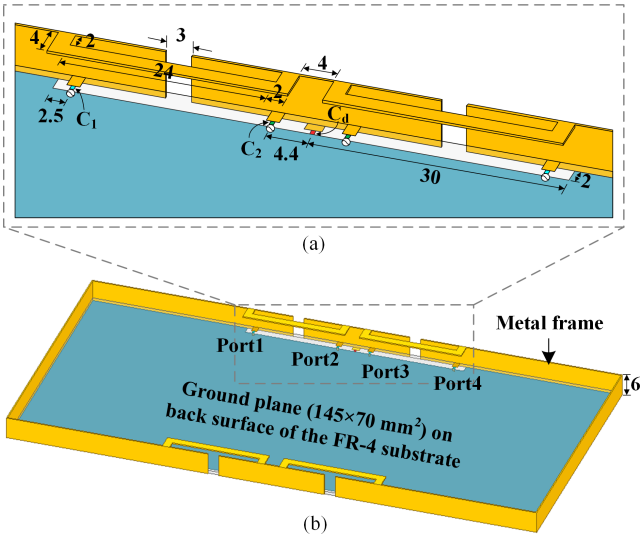

Fig. 9. Geometry of the (a) integrated quad-element configuration and (b) 8 × 8 MIMO antenna system, C_1 = 0.6 pF, C_2 = 0.7 pF, and C_d = 1.8 pF, unit all in millimeters.

"Case I." On the contrary, when we put two sets of back-to-back antenna pairs together, the arrangement of two central elements is exactly the face-to-face configuration, so we can suppress the coupling of two central elements by a capacitance, as shown in Fig. 8(d). Consequently, another integrated quad-element configuration is also realized, which is defined as "Case II." Based on the wideband decoupling performance of the complementary antenna pairs, both Case I and Case II can realize isolation of better than 10 dB between all four elements across a wide bandwidth of 3.3–5.0 GHz.

B. 8 × 8 MIMO Antenna System

Since Case II has fewer frame slots (two frame slots) than that of Case I (three frame slots), so we choose Case II as a design example to validate the concept of the proposed integrated quad-element design scheme. As shown in Fig. 9, by using two such integrated quad-element structures (Case II) along two side edges of the smartphone casing, an 8 × 8 MIMO system can be implemented. The ground plane, with a dimension of 145 × 70 mm^2, is printed on the back surface of the FR-4 substrate. Two 60 × 2 mm^2 slots are etched at the ground plane. A full circle of the metal frame has vertically surrounded the mainboard and connected with the ground plane. Only two frame slots are etched for each integrated quad-element configuration. At each feeding port, a lumped capacitance (C_1 for port1 and port4, C_2 for port2 and port3) is connected in series for impedance matching. The left connecting line is used for the decoupling between port1 and port2, while the right one is used for the decoupling between port3 and port4. The coupling between port2 and port3 is reduced by the capacitance C_d.

As shown in Fig. 10, a prototype is fabricated to verify the feasibility. The mainboard is manufactured by 145 × 70 × 0.8 mm^3 FR-4 substrate through a standard printed circuit board process. The metal frame and the connecting lines are integrated processing and are manufactured by 0.3 mm-thick brass plates through laser cutting process. For ease of fabrication, the two decoupling lines are connected, which does not affect the antenna performance. Eight 50 Ω SMA connectors and eight 50 Ω microstrip feedlines are used to excite eight ports for antenna test.

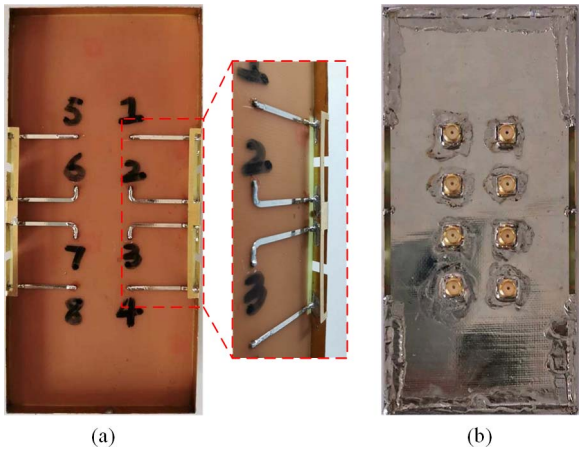

Fig. 10. Photograph of the fabricated 8 × 8 MIMO antenna system. (a) Top view: inset is the enlarged view of the integrated quad-element configuration. (b) Bottom view.

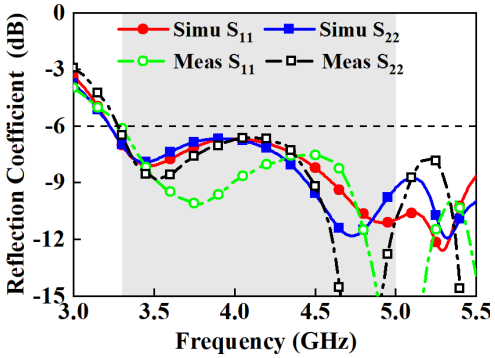

Fig. 11. Simulated and measured reflection coefficients of the 8 × 8 MIMO system.

C. Simulated and Measured Results

The simulated and measured reflection coefficients of the 8 × 8 MIMO system are presented in Fig. 11. Due to the symmetrical structure, only the results of port1 and port2 are presented for brevity. As seen, both the simulated and measured results show a good impedance matching of better than −6 dB across 3.3–5.0 GHz and even beyond. The measured result slightly disagrees with the simulated result due to the manual fabrication error of the metal frame, which can be reduced in practical mass production.

The simulated and measured isolation of the integrated quad-element MIMO antenna is proposed in Fig. 12. The simulated result is in line with the measured result. Both the simulated and measured isolations are better than 10 dB across 3.3–5.0 GHz with the help of the proposed hybrid wideband decoupling methods. The simulated and measured isolations between two sets of integrated quad-element MIMO antennas are reported in Fig. 13(a) and (b), respectively, which are better than 17.7 and 18.7 dB due to the spatial diversity.

The surface current distribution is analyzed in Fig. 14 to provide an intuitive insight into the decoupling performance. When fed through port1, the odd mode of the connecting

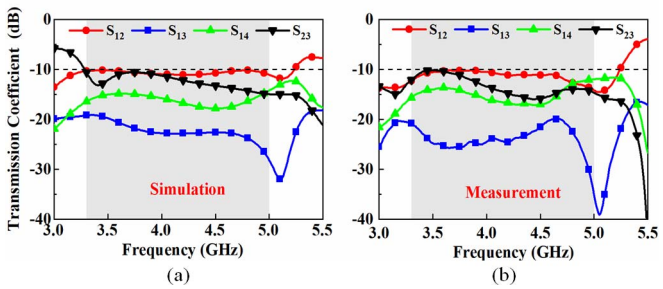

Fig. 12. (a) Simulated and (b) measured isolations for the integrated quad-element MIMO antenna.

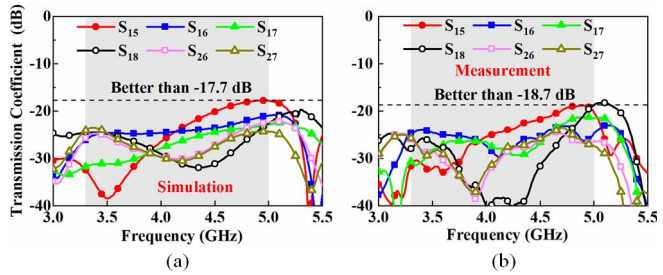

Fig. 13. (a) Simulated and (b) measured isolations between two sets of integrated quad-element MIMO antennas.

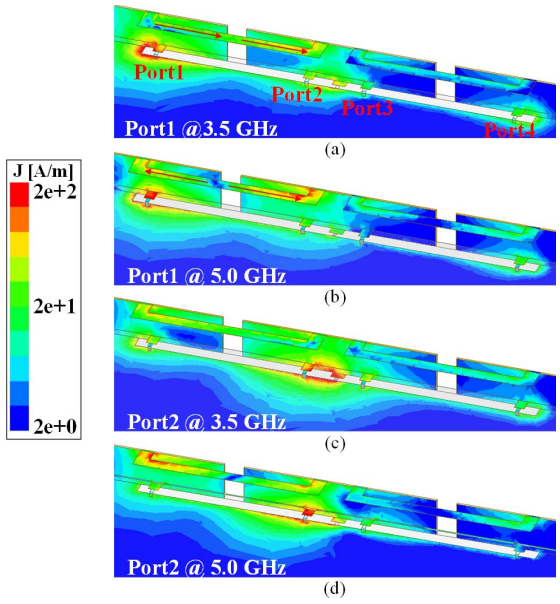

Fig. 14. Simulated current distributions. (a) Port1 feed at 3.5 GHz. (b) Port1 feed at 5.0 GHz. (c) Port2 feed at 3.5 GHz. (d) Port2 feed at 5.0 GHz.

line is excited in the lower band, whereas the even mode is excited in the higher band. Hence, a wide decoupling bandwidth between port1 and port2 can be realized by the dual-mode decoupling of the connecting line [40]. When fed through port2, the coupling current to port3 is "short-circuited" in the lower band due to the series *LC* tank, whereas the coupling current is weak in the higher band due to the localized resonance of open-slot elements. Therefore, a wide decoupling bandwidth between port2 and port3 can be realized by the capacitance. Symmetric current distributions can also be observed when fed through port3 and port4, which is not shown for brevity.

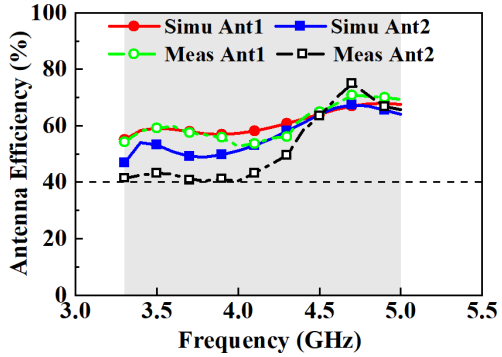

Fig. 15. Simulated and measured efficiency of the 8 × 8 MIMO system.

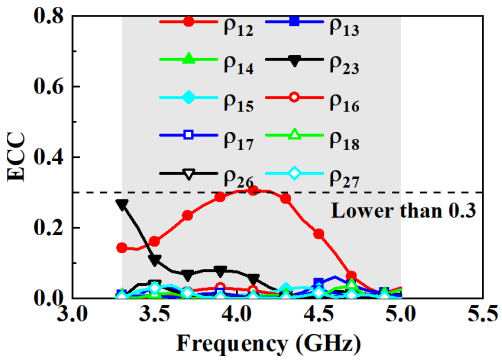

Fig. 16. ECC calculated by the measured far field of the 8 × 8 MIMO system.

The simulated and measured total antenna efficiency is proposed in Fig. 15. The simulated efficiency is 55.2%–68.0% for Ant1 and 47.0%–67.5% for Ant2, while the measured efficiency is 52.8%–70.8% for Ant1 and 40.5%–75.0% for Ant2. The slight inconsistency between the simulated and measurement results is caused by the manual fabrication error of the metal frame. The mutual coupling of adjacent antenna elements will degenerate the antenna efficiency. Since Ant1 is only adjacent to Ant2, but Ant2 is adjacent to both Ant1 and Ant3, so the efficiency of Ant2 is lower than Ant1.

To demonstrate the diversity performance of the 8 × 8 MIMO system, the ECC calculated by the measured far-field is plotted in Fig. 16. As seen, the ECCs between adjacent elements are worse than that between nonadjacent elements. The ECCs between any two ports are lower than 0.3 across 3.3–5.0 GHz, which can satisfy the standards in smartphones.

D. Comparison

To highlight the merits of the proposed design scheme, a comparison table (Table II) is proposed to compare this work with the existing integrated quad-element MIMO antennas for 5G smartphones. As seen, the antenna bandwidth is dramatically improved from less than 200 MHz in [41] and [42] to 1700 MHz by multimode resonance and wideband decoupling techniques, thereby covering the entire 5G N77, N78, and N79 bands. In addition, the antennas are co-designed with the metal frame of smartphones, which can be directly applied to mainstream smartphones without additional consideration of the impact of the metal frame. Besides, the antenna efficiency is also better than that in [41] and [42]. Consequently, the proposed antenna shows the advantages of wide bandwidth,

TABLE II
COMPARISON OF THE INTEGRATED QUAD-ELEMENT MIMO ANTENNA

Ref	Metal Frame	Bandwidth (GHz)	Size of Quad-Ant. (mm^2)	Isolation	Efficiency
[41]	×	3.4~3.6	50×3	>10 dB	52.0~60.0% 40.0~50.0%
[42]	×	3.6~3.74	40.8×3	>11.6 dB	29.0~38.5% 41.5~44.9%
Our work	√	3.3~5.0	60×2	>10 dB	52.8~70.8% 40.5~75.0%

high efficiency, and metal frame compatibility over the existing integrated quad-antenna design scheme, which is a good candidate for future highly-integrated 5G MIMO antennas.

IV. IMPACTS OF USER'S HANDS

To analyze the impacts of the user's hands on the antenna performance, the proposed 8 × 8 MIMO antenna with single-handed and two-handed handhold models, are simulated and analyzed in CST microwave studio.

For the single-handed handhold mode, as shown in Fig. 17(a), the fingers of hand phantom touch on antenna elements over a large area. The simulated reflection coefficient, isolation, and total efficiency in the single-handed mode are illustrated in Fig. 17(b)–(d), respectively. As seen, the impedance matching and isolation of most ports are almost unchanged with the hand phantom. The impedance matching of Ant3 and Ant4 are improved due to the absorption of the user's hand, and the isolation between Ant3 and Ant4 is slightly diminished to 7.8 dB. However, the antenna efficiency is significantly deteriorated due to the high absorption loss of the user's hand. For the antenna elements near to the fingers of the hand phantom, such as Ant2, Ant3, Ant4, and Ant8, the antenna efficiency is decreased by 20%–35%.

For the two-handed handhold mode, as shown in Fig. 17(e), the fingers of the hand phantom can hardly touch the antenna elements. The simulated reflection coefficient, isolation, and total efficiency in the two-handed mode are illustrated in Fig. 17(f)–(h), respectively. It can be seen that the impedance characteristics of all ports almost keep unchanged. The antenna efficiency of Ant1–4 is hardly affected by the user's hand, but the antenna efficiency of Ant 5–8 are significantly deteriorated by about 30% due to the radiation energy absorption of user's fingers.

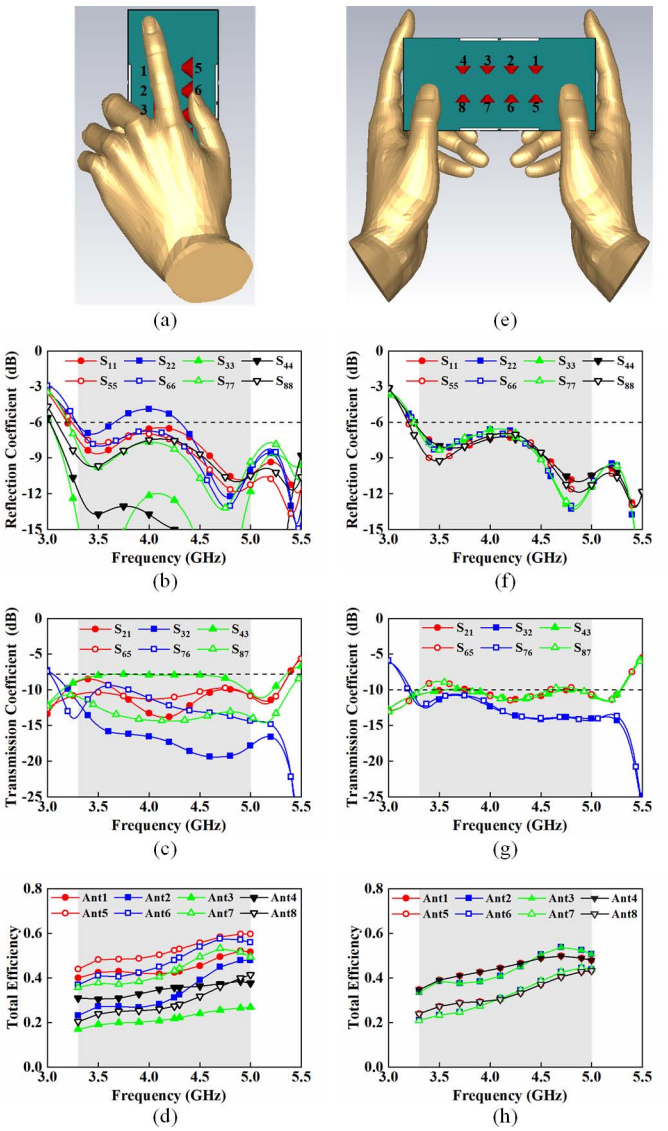

Fig. 17. Simulated antenna performance with user's hand effects in the single-handed and two-handed scenarios. (a)–(d) Single-handed scenario and the corresponding reflection coefficient, transmission coefficient, and total efficiency. (e)–(h) Two-handed scenario and the corresponding reflection coefficient, transmission coefficient, and total efficiency.

V. EXTENSION TO INTEGRATED MULTIANTENNA CONFIGURATIONS

In addition to the integrated quad-antenna configuration, flexible extension to integrated multiantenna configuration with arbitrary element number can also be implemented based on the complementary antenna pairs. For example, the conceptual diagram of the integrated six-antenna and eight-antenna configurations is illustrated in Fig. 18(a) and (b), respectively. The integrated six-antenna configuration consists of three sets of back-to-back antenna pairs and is decoupled by lumped capacitances between the pairs. Alternatively, the integrated six-antenna configuration can also be constituted by three sets of face-to-face antenna pair and decoupled by two connecting lines between the pairs, just as the extension of that in Fig. 8(c), which is not shown for brevity. Furthermore, it can be further extended to higher-order configurations, such as integrated eight-antenna configuration as shown in Fig. 18(b). The simulation model of the integrated eight-antenna configuration is proposed in Fig. 18(c), and the corresponding simulated S-parameters are demonstrated in Fig. 18(d) and (e). As seen, all antenna elements have a good impedance matching of better than −6 dB across 3.3–5.0 GHz, and a good isolation of better than 9.5 dB between adjacent elements is also achieved. By this way, a 16 × 16 MIMO system can be readily achieved by placing two sets of integrated eight-antenna configurations along two side edges of the smartphone, which paves the way for future higher-order MIMO systems in smartphones.

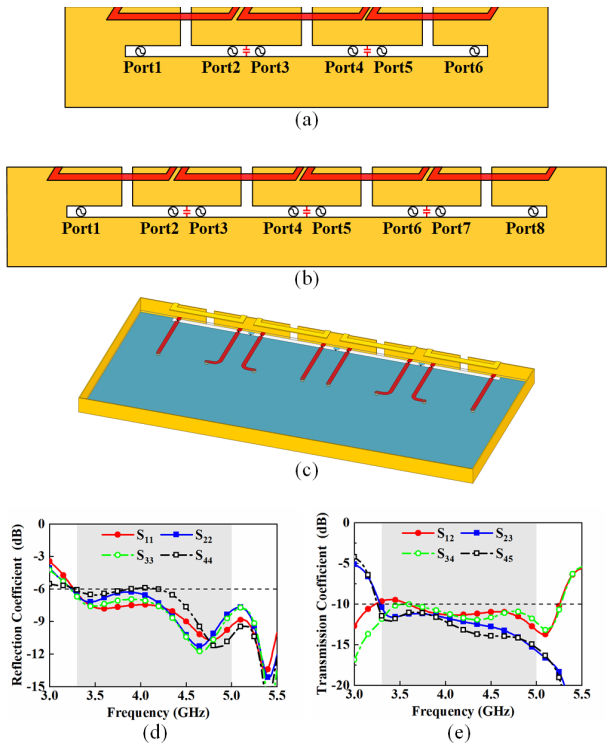

Fig. 18. Extension to integrated multiantenna configurations. Conceptual diagram of the (a) integrated six-antenna and (b) integrated eight-antenna configurations. (c) Simulation model of the integrated eight-antenna configuration and the corresponding simulated (d) reflection coefficients and (e) isolations between adjacent antenna elements.

VI. Conclusion

This article proposes a highly-integrated wideband MIMO antenna design scheme for the size-limited 5G smartphones. First, the wideband decoupling of two closely-spaced open-slot antennas in face-to-face and back-to-back configurations is investigated. The face-to-face antenna pair shows a wide bandwidth of 3.3–7.2 GHz within a compact size of 24 × 2 × 5 mm^3. Based on the complementary antenna pairs, an integrated quad-element MIMO antenna with a compact footprint of 60 × 2 × 6 mm^3 is proposed. Then, by placing two sets of integrated quad-element MIMO antennas in smartphone casing, an 8 × 8 MIMO system is implemented. Both the simulated and measured results show that the 8 × 8 MIMO system could offer a bandwidth of 3.3–5.0 GHz with impedance matching better than −6 dB and isolations above 10 dB. Acceptable antenna efficiency of 52.8%–70.8% and 40.5%–75.0% is also realized for the 8 × 8 MIMO system. In addition to the integrated quad-antenna design, flexible extension to integrated multiantenna design is also discussed for future higher-order MIMO application. We forecast that the proposed design scheme, with the merits of high integration level, wide bandwidth, and flexible configurations, has the potential for the application of future 5G smartphones.

References

[1] J. G. Andrews *et al.*, "What will 5G be?" *IEEE J. Sel. Areas Commun.*, vol. 32, no. 6, pp. 1065–1082, Jun. 2014.

[2] G. J. Foschini and M. J. Gans, "On limits of wireless communications in a fading environment when using multiple antennas," *Wireless Pers. Commun.*, vol. 6, no. 3, pp. 311–335, Mar. 1998.

[3] A. A. Al-Hadi, J. Ilvonen, R. Valkonen, and V. Viikari, "Eight-element antenna array for diversity and MIMO mobile terminal in LTE 3500 MHz band," *Microw. Opt. Technol. Lett.*, vol. 56, no. 6, pp. 1323–1327, Jun. 2014.

[4] K.-L. Wong and J.-Y. Lu, "3.6-GHz 10-antenna array for MIMO operation in the smartphone," *Microw. Opt. Technol. Lett.*, vol. 57, no. 7, pp. 1699–1704, Jul. 2015.

[5] Y.-L. Ban, C. Li, C.-Y.-D. Sim, G. Wu, and K.-L. Wong, "4G/5G multiple antennas for future multi-mode smartphone applications," *IEEE Access*, vol. 4, pp. 2981–2988, Jul. 2016.

[6] M.-Y. Li *et al.*, "Eight-port orthogonally dual-polarized antenna array for 5G smartphone applications," *IEEE Trans. Antennas Propag.*, vol. 64, no. 9, pp. 3820–3830, Sep. 2016.

[7] H. Xu, H. Zhou, S. Gao, H. Wang, and Y. Cheng, "Multimode decoupling technique with independent tuning characteristic for mobile terminals," *IEEE Trans. Antennas Propag.*, vol. 65, no. 12, pp. 6739–6751, Dec. 2017.

[8] J. Guo, L. Cui, C. Li, and B. Sun, "Side-edge frame printed eight-port dual-band antenna array for 5G smartphone applications," *IEEE Trans. Antennas Propag.*, vol. 66, no. 12, pp. 7412–7417, Dec. 2018.

[9] X. Zhao, S. P. Yeo, and L. C. Ong, "Decoupling of inverted-F antennas with high-order modes of ground plane for 5G mobile MIMO platform," *IEEE Trans. Antennas Propag.*, vol. 66, no. 9, pp. 4485–4495, Sep. 2018.

[10] Q. Chen *et al.*, "Single ring slot-based antennas for metal-rimmed 4G/5G smartphones," *IEEE Trans. Antennas Propag.*, vol. 67, no. 3, pp. 1476–1487, Mar. 2019.

[11] D. Huang, Z. Du, and Y. Wang, "Slot antenna array for fifth generation metal frame mobile phone applications," *Int. J. RF Microw. Comput.-Aided Eng.*, vol. 29, no. 9, Sep. 2019, Art. no. e21841.

[12] W. Jiang, B. Liu, Y. Cui, and W. Hu, "High-isolation eight-element MIMO array for 5G smartphone applications," *IEEE Access*, vol. 7, pp. 34104–34112, 2019.

[13] Y. Li, Y. Luo, and G. Yang, "High-isolation 3.5 GHz eight-antenna MIMO array using balanced open-slot antenna element for 5G smartphones," *IEEE Trans. Antennas Propag.*, vol. 67, no. 6, pp. 3820–3830, Jun. 2019.

[14] X. Zhang, Y. Li, W. Wang, and W. Shen, "Ultra-wideband 8-Port MIMO antenna array for 5G metal-frame smartphones," *IEEE Access*, vol. 7, pp. 72273–72282, 2019.

[15] A. Zhao and Z. Ren, "Size reduction of self-isolated MIMO antenna system for 5G mobile phone applications," *IEEE Antennas Wireless Propag. Lett.*, vol. 18, no. 1, pp. 152–156, Jan. 2019.

[16] A. Zhao and Z. Ren, "Wideband MIMO antenna systems based on coupled-loop antenna for 5G N77/N78/N79 applications in mobile terminals," *IEEE Access*, vol. 7, pp. 93761–93771, 2019.

[17] D. Q. Liu, H. J. Luo, M. Zhang, H. L. Wen, B. Wang, and J. Wang, "An extremely low-profile wideband MIMO antenna for 5G smartphones," *IEEE Trans. Antennas Propag.*, vol. 67, no. 9, pp. 5772–5780, Sep. 2019.

[18] D. Huang, Z. Du, and Y. Wang, "Eight-band antenna for full-screen metal frame LTE mobile phones," *IEEE Trans. Antennas Propag.*, vol. 67, no. 3, pp. 1527–1534, Mar. 2019.

[19] C.-Z. Han *et al.*, "A frequency-reconfigurable antenna with 1-mm nonground portion for metal-frame and full-display screen handset applications using mode control method," *IEEE Access*, vol. 7, pp. 48037–48045, Apr. 2019.

[20] J. Choi, W. Hwang, C. You, B. Jung, and W. Hong, "Four-element reconfigurable coupled loop MIMO antenna featuring LTE full-band operation for metallic-rimmed smartphone," *IEEE Trans. Antennas Propag.*, vol. 67, no. 1, pp. 99–107, Jan. 2019.

[21] K.-L. Wong, C.-Y. Tsai, and J.-Y. Lu, "Two asymmetrically mirrored gap-coupled loop antennas as a compact building block for eight-antenna MIMO array in the future smartphone," *IEEE Trans. Antennas Propag.*, vol. 65, no. 4, pp. 1765–1778, Apr. 2017.

[22] K.-L. Wong, B.-W. Lin, and W.-Y. Li, "Dual-band dual inverted-F/loop antennas as a compact decoupled building block for forming eight 3.5/5.8-GHz MIMO antennas in the future smartphone," *Microw. Opt. Technol. Lett.*, vol. 59, no. 11, pp. 2715–2721, Nov. 2017.

[23] Z. Ren, A. Zhao, and S. Wu, "MIMO antenna with compact decoupled antenna pairs for 5G mobile terminals," *IEEE Antennas Wireless Propag. Lett.*, vol. 18, no. 7, pp. 1367–1371, Jul. 2019.

[24] Z. Ren and A. Zhao, "Dual-band MIMO antenna with compact self-decoupled antenna pairs for 5G mobile applications," *IEEE Access*, vol. 7, pp. 82288–82296, 2019.

[25] K. L. Wong, Y. H. Chen, and W. Y. Li, "Decoupled compact ultra-wideband MIMO antennas covering 3300∼6000 MHz for the fifth-generation mobile and 5GHz-WLAN operations in the future smartphone," *Microw. Opt. Technol. Lett.*, vol. 60, pp. 2345–2351, Oct. 2018.

[26] C. Deng, "Compact broadband multi-input multi-output antenna covering 3300 to 6000 MHz band for 5G mobile terminal applications," *Microw. Opt. Technol. Lett.*, vol. 62, no. 10, pp. 3310–3316, Oct. 2020.
[27] K.-L. Wong, B.-W. Lin, and S.-E. Lin, "High-isolation conjoined loop multi-input multi-output antennas for the fifth-generation tablet device," *Microw. Opt. Technol. Lett.*, vol. 61, no. 1, pp. 111–119, Jan. 2019.
[28] J. Sui, Y. Dou, X. Mei, and K.-L. Wu, "Self-curing decoupling technique for MIMO antenna arrays in mobile terminals," *IEEE Trans. Antennas Propag.*, vol. 68, no. 2, pp. 838–849, Feb. 2020.
[29] L. Sun, H. Feng, Y. Li, and Z. Zhang, "Compact 5G MIMO mobile phone antennas with tightly arranged orthogonal-mode pairs," *IEEE Trans. Antennas Propag.*, vol. 66, no. 11, pp. 6364–6369, Nov. 2018.
[30] L. Sun, H. Feng, Y. Li, and Z. Zhang, "Tightly arranged orthogonal mode antenna for 5G MIMO mobile terminal," *Microw. Opt. Technol. Lett.*, vol. 60, no. 7, pp. 1751–1756, Jul. 2018.
[31] H. Xu, S. S. Gao, H. Zhou, H. Wang, and Y. Cheng, "A highly integrated MIMO antenna unit: Differential/common mode design," *IEEE Trans. Antennas Propag.*, vol. 67, no. 11, pp. 6724–6734, Nov. 2019.
[32] Z. Xu and C. Deng, "High-isolated MIMO antenna design based on pattern diversity for 5G mobile terminals," *IEEE Antennas Wireless Propag. Lett.*, vol. 19, no. 3, pp. 467–471, Mar. 2020.
[33] L. Chang, Y. Yu, K. Wei, and H. Wang, "Polarization-orthogonal co-frequency dual antenna pair suitable for 5G MIMO smartphone with metallic bezels," *IEEE Trans. Antennas Propag.*, vol. 67, no. 8, pp. 5212–5220, Aug. 2019.
[34] A. Ren, Y. Liu, and C.-Y.-D. Sim, "A compact building block with two shared-aperture antennas for eight-antenna MIMO array in metal-rimmed smartphone," *IEEE Trans. Antennas Propag.*, vol. 67, no. 10, pp. 6430–6438, Oct. 2019.
[35] C.-Z. Han, L. Xiao, Z. Chen, and T. Yuan, "Co-located self-neutralized handset antenna pairs with complementary radiation patterns for 5G MIMO applications," *IEEE Access*, vol. 8, pp. 73151–73163, 2020.
[36] L. Chang, Y. Yu, K. Wei, and H. Wang, "Orthogonally polarized dual antenna pair with high isolation and balanced high performance for 5G MIMO smartphone," *IEEE Trans. Antennas Propag.*, vol. 68, no. 5, pp. 3487–3495, May 2020.
[37] H. Piao, Y. Jin, and L. Qu, "A compact and straightforward self-decoupled MIMO antenna system for 5G applications," *IEEE Access*, vol. 8, pp. 129236–129245, 2020.
[38] L. Sun, Y. Li, Z. Zhang, and Z. Feng, "Wideband 5G MIMO antenna with integrated orthogonal-mode dual-antenna pairs for metal-rimmed smartphones," *IEEE Trans. Antennas Propag.*, vol. 68, no. 4, pp. 2494–2503, Apr. 2020.
[39] L. Sun, Y. Li, Z. Zhang, and H. Wang, "Self-decoupled MIMO antenna pair with shared radiator for 5G smartphones," *IEEE Trans. Antennas Propag.*, vol. 68, no. 5, pp. 3423–3432, May 2020.
[40] L. Sun, Y. Li, and Z. Zhang, "Wideband decoupling of integrated slot antenna pairs for 5G smartphones," *IEEE Trans. Antennas Propag.*, early access, Sep. 11, 2020, doi: 10.1109/TAP.2020.3021785.
[41] K.-L. Wong, J.-Y. Lu, L.-Y. Chen, W.-Y. Li, and Y.-L. Ban, "8-antenna and 16-antenna arrays using the quad-antenna linear array as a building block for the 3.5-GHz LTE MIMO operation in the smartphone," *Microw. Opt. Technol. Lett.*, vol. 58, no. 1, pp. 174–181, Jan. 2016.
[42] C. Deng, D. Liu, and X. Lv, "Tightly arranged four-element MIMO antennas for 5G mobile terminals," *IEEE Trans. Antennas Propag.*, vol. 67, no. 10, pp. 6353–6361, Oct. 2019.
[43] Z. Zhang, *Antenna Design for Mobile Devices*, 2nd ed. Hoboken, NJ, USA: Wiley, 2017.
[44] D. M. Pozar, *Microwave Engineering*, 2nd ed. New York, NY, USA: Wiley, 1998.
[45] R. G. Vaughan and J. B. Andersen, "Antenna diversity in mobile communications," *IEEE Trans. Veh. Technol.*, vol. VT-36, no. 4, pp. 147–172, Nov. 1987.

Libin Sun (Graduate Student Member, IEEE) was born in Ningbo, China, in 1994. He received the B.S. degree from Xidian University, Xi'an, China, in 2016. He is currently pursuing the Ph.D. degree with the Department of Electronic Engineering, Tsinghua University, Beijing, China.

His current research interests include antenna design and theory, particularly in 5G mobile phone antennas, antenna decoupling, multiple-input multiple-output (MIMO) and diversity antennas, circularly-polarized antennas, leaky-wave antennas, and surface-wave antennas.

Mr. Sun was a recipient of the Top Reviewer Award for the IEEE TRANSACTIONS ON ANTENNAS AND PROPAGATION in 2019 and the Honorable Mention at the Student Paper Competition of the 2020 IEEE AP-S Conference. He has served as the Session Chair for the IEEE APMC 2020. He serves as a reviewer for several international academic journals such as the IEEE TRANSACTIONS ON ANTENNAS AND PROPAGATION, IEEE ANTENNAS AND WIRELESS PROPAGATION LETTERS, IEEE ACCESS, *IET Microwaves, Antennas & Propagation*, *IET Electronics Letters*, and *Microwave and Optical Technology Letters*.

Yue Li (Senior Member, IEEE) received the B.S. degree in telecommunication engineering from Zhejiang University, Hangzhou, China, in 2007, and the Ph.D. degree in electronic engineering from Tsinghua University, Beijing, China, in 2012.

In June 2012, he was a Post-Doctoral Fellow with the Department of Electronic Engineering, Tsinghua University. In December 2013, he was a Research Scholar with the Department of Electrical and Systems Engineering, University of Pennsylvania, Philadelphia, PA, USA. He was also a Visiting Scholar with the Institute for Infocomm Research (I2R), A∗STAR, Singapore, in 2010, and the Hawaii Center of Advanced Communication (HCAC), University of Hawai'i at Mānoa, Honolulu, HI, USA, in 2012. Since January 2016, he has been with Tsinghua University, where he is currently an Assistant Professor and also an Associate Professor with the Department of Electronic Engineering. He has authored or coauthored over 130 journal articles and 45 international conference papers, and holds 18 granted Chinese patents. His current research interests include metamaterials, plasmonics, electromagnetics, nanocircuits, mobile and handset antennas, multiple-input multiple-output (MIMO) and diversity antennas, and millimeter-wave antennas and arrays.

Dr. Li was a recipient of the Issac Koga Gold Medal from URSI General Assembly in 2017; the Second Prize of Science and Technology Award of China Institute of Communications in 2017; the young scientist awards from the conferences of ACES 2018, AT-RASC 2018, AP-RASC 2016, EMTS 2016, and URSI GASS 2014; the best paper awards from the conferences of CSQRWC 2018, NCMMW 2018 and 2017, APCAP 2017, NCANT 2017, ISAPE 2016, and ICMMT 2016; the Outstanding Doctoral Dissertation of Beijing Municipality in 2013; and the Principal Scholarship of Tsinghua University in 2011. He is serving as an Associate Editor for IEEE TRANSACTIONS ON ANTENNAS AND PROPAGATION, IEEE ANTENNAS AND WIRELESS PROPAGATION LETTERS, and *Computer Applications in Engineering Education*, and also the Editorial Board of Scientific Report.

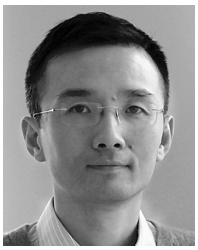

Zhijun Zhang (Fellow, IEEE) received the B.S. and M.S. degrees from the University of Electronic Science and Technology of China, Chengdu, China, in 1992 and 1995, respectively, and the Ph.D. degree from Tsinghua University, Beijing, China, in 1999.

In 1999, he joined the Department of Electrical Engineering, The University of Utah, Salt Lake City, UT, USA, as a Post-Doctoral Fellow, where he was appointed as a Research Assistant Professor in 2001. In May 2002, he joined the University of Hawai'i at Mānoa, Honolulu, HI, USA, as an Assistant Researcher. In November 2002, he joined Amphenol T&M Antennas, Vernon Hills, IL, USA, as a Senior Staff Antenna Development Engineer and then was promoted to the position of Antenna Engineer Manager. In 2004, he joined Nokia Inc., San Diego, CA, USA, as a Senior Antenna Design Engineer. In 2006, he joined Apple Inc., Cupertino, CA, as a Senior Antenna Design Engineer and then was promoted to the position of Principal Antenna Engineer. Since August 2007, he has been with Tsinghua University, where he is currently a Professor with the Department of Electronic Engineering. He has authored *Antenna Design for Mobile Devices* (Wiley, 1st ed. 2011, 2nd ed. 2017).

Dr. Zhang served as an Associate Editor for the IEEE TRANSACTIONS ON ANTENNAS AND PROPAGATION from 2010 to 2014 and the IEEE ANTENNAS AND WIRELESS PROPAGATION LETTERS from 2009 to 2015.